Infrared reflectivity and Raman scattering in GeS

J. D. Wiley,*† W. J. Buckel,‡ and R. L. Schmidt
Max-Planck-Institut für Festkörperforschung, Stuttgart, Federal Republic of Germany
(Received 4 August 1975)

Zone-center optical phonons have been measured using infrared reflectivity and Raman scattering for single-crystal, orthombic GeS. Using Kramers-Kronig analysis and oscillator fits of the reflectivity data, we have determined the infrared-active TO and associated LO phonon frequencies, and dielectric constants for all three principal polarizations. Group-theoretical analysis of the three-dimensional space group of GeS (D_{2h}^{16}) predicts seven infrared-active phonons. Only six of these were observed. Raman measurements yielded an additional 12 zone-center phonons (in agreement with theoretical predictions). Despite the fact that GeS possesses a center of inversion symmetry, many of the infrared and Raman modes are found to be nearly degenerate. This is taken as evidence for the importance of the diperiodic layer symmetry (DG32, no inversion center) in determining the vibrational properties of GeS. The ratios of various *intralayer* to *interlayer* force constants are estimated and found to lie in the range 12:1 to 30:1.

I. INTRODUCTION

The preparation of good-quality, single-crystal GeS was first reported by Yambumoto[1] in 1958 and there have been a few papers on the physical properties of crystalline GeS since that time.[2–10] Nevertheless, GeS remains the least studied member of the group IV-VI semiconductors and, until quite recently, remarkably little was known about it other than its crystal structure, the approximate magnitude of the band gap, and the fact that it exhibits photoconduction. This is perhaps surprising, since GeS occupies a very interesting position among the compound semiconductors. It is one of the few compound semiconductors which is easily produced in both crystalline and amorphous forms[8]; it is the least anisotropic member of the series of orthorhombic IV-VI semiconductors: GeS, GeSe, SnS, and SnSe,[11] and , as will be shown here and in a forthcoming publication,[12] it behaves as if it were in some sense an intermediate case between the interesting two-dimensional (layer-type) and three-dimensional crystals. In the present paper, we report the results of infrared-reflectivity and Raman-scattering measurements on single-crystal GeS as a contribution to the understanding of its lattice vibrations. The emphasis in this paper will be on experimental results, with theoretical interpretation and a model for the lattice dynamics being deferred to a forthcoming publication.[12]

GeS is a semiconductor with a direct band gap of $E_g = 1.65$, 1.737, and 1.744 eV at 300, 77, and 4.2 °K, respectively.[10] Although the magnitude of the band gap appears to be isotropic, the absorption edge is highly anisotropic, being direct allowed for $\vec{E} \| \vec{a}$ and $\vec{E} \| \vec{c}$ directions, and forbidden for $\vec{E} \| \vec{b}$. It crystallizes in an orthorhombic (space group D_{2h}^{16}) structure with eight atoms per unit cell and lattice constants[1,2,11,13] $a = 4.30$ Å, $b = 3.65$ Å, and $c = 10.44$ Å. This lattice structure can be viewed as a distortion of the NaCl structure, the distortion being such as to form double-layer planes perpendicular to the c axis.[11] Each atom has three strongly bonded neighbors within its own layer and three more distant (weakly bonded) neighbors, one of which lies in an adjacent layer. Because of the weak interlayer bonding, GeS exhibits exceptionally easy cleavage perpendicular to the c axis, leading one to expect that it may show some features characteristic of two-dimensional or "layer-type" compounds. It is just this question of the degree to which GeS exhibits two-dimensional behavior in its lattice vibrational properties that we wish to address in this and a subsequent publication.[12]

It is well known[14,15] that a careful comparison of the infrared and Raman-active phonon energies energies can yield valuable information about interlayer force constants in layer-type semiconductors. Central to this analysis is the recognition that there are two relevant symmetries in the case of layer-type materials: the space-group symmetry of the three-dimensional crystal, and the diperiodic symmetry[16] of an individual layer. We do not propose to give here a complete group-theoretic analysis of the lattice vibrations in GeS, but a brief summary of the main conclusions[12] will prove useful in cataloging the measured phonons.

The three-dimensional space group of the GeS lattice is, as already mentioned, D_{2h}^{16}. There is a center of inversion symmetry in this lattice (lying between the layers) so that one should expect the infrared and Raman-active phonons to be distinct (nondegenerate). On the other hand, the relevant diperiodic group (DG32 in Woods notation[16]—the diperiodic analog of the triperiodic group C_{2v}^7) has no inversion center. Thus, to the extent that the vibrational properties of GeS are

dominated by *intralayer* forces, one should expect degeneracies or near degeneracies between some of the infrared and Raman-active phonons, with splittings depending on the strength of the interlayer forces. In the present paper, we will classify the observed phonons in terms of their three-dimensional symmetries. A factor-group analysis of the group D_{2h}^{16} reveals that, of the 21 optical phonons, 2 are inactive, 7 are infrared active, and 12 are Raman active. Figure 1 summarizes these phonons, their symmetries and the experimental conditions necessary for their observation, and shows the compatability relations which exist between phonons for the DG32 and D_{2h}^{16} symmetries.[17]

Section II contains details of the experimental measurements together with infrared and Raman spectra. Section III contains a discussion of the Kramers-Kronig analysis and oscillator fits necessary to deduce phonon energies from the infrared reflectivity, along with a brief discussion of the infrared-Raman splittings. In Sec. IV, we summarize our results and conclusions.

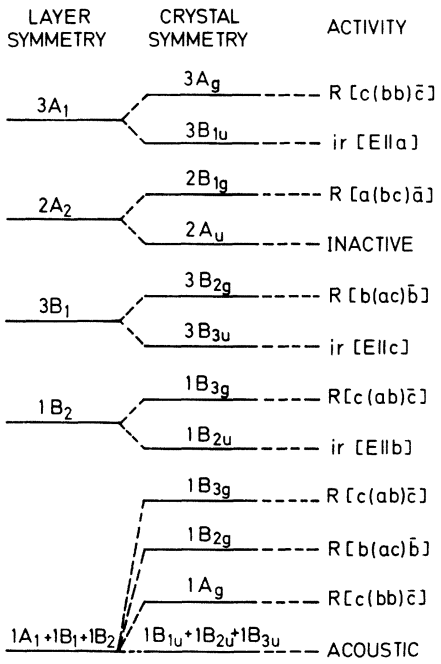

FIG. 1. Diagram showing the relations among phonons for individual layers and three dimensional crystals of GeS. The column on the left, labeled "Layer Symmetry" assumes two adjacent but decoupled layers of Ges with diperiodic symmetry (Ref. 16) DG32. Degeneracies given in this column are *per layer*. In the presence of interlayer coupling, the phonons are split as shown and labelled in accordance with the GeS space group D_{2h}^{16}. The optical activities (*R* for Raman and ir for infrared) of these phonons and experimental conditions necessary for their observation are shown on the right-hand side. The vertical scale is not intended to represent an ordering in energy.

II. EXPERIMENTAL

A. Samples

Details of the growth of the crystals used in this study have already been published elsewhere.[18] Briefly, polycrystalline GeS was first synthesized from high purity elemental Ge and S, and transferred to quartz ampoules which were evacuated and sealed. No intentional dopants were added. Crystals were then grown by slow sublimation, resulting in single-crystal ingots 1.75 cm in diameter and 4–5 cm in length. For measurements involving *c* faces (i.e., faces perpendicular to the *c* axis[13]), sample preparation was trivial because of the easy cleavage in this plane. All measurements on *c* faces were made with freshly cleaved surfaces prepared by simply peeling off a 5–10-μm layer with cellophane tape. The *a* and *b* axes were located within a cleavage face from conventional Laue photographs. Samples intended for measurements on *a* and *b* faces were more difficult to prepare since these required cutting and polishing perpendicular to the cleavage planes. This was accomplished by first cutting the samples in the correct orientation using a diamond-impregnated wire saw, and then fastening them to glass slides with epoxy prior to polishing. In most cases, this prevented the samples from falling apart during polishing. The polishing itself was done very gently, using aqueous suspensions of Al_2O_3 on polishing cloths. Surfaces prepared in this manner were entirely adequate for infrared reflectivity measurements, although they were visibly inferior to the mirrorlike cleaved faces. For the Raman measurements, it was found advantageous to give the *a* and *b* faces a final light polish with Syton[19] immediately prior to measurement.

B. Infrared reflectivity measurements

Figure 2 shows the results of infrared-reflectivity measurements at 300 °K in a frequency range from 20 to 450 cm^{-1}. These measurements were performed on a Polytec FIR 30 Fourier spectrometer with a resolution of 2.5 cm^{-1}. The spectra for $\vec{E}\|\vec{a}$ and $\vec{E}\|\vec{b}$ were taken on an oriented cleavage face using a wire-grid polarizer which could be rotated by 90° for recording the two spectra. Owing to the large anisotropy of GeS, it is necessary to perform this alignment quite carefully. In the present measurements, we saw no trace of the sharp 120-cm^{-1} $\vec{E}\|\vec{a}$ resonance when recording the $\vec{E}\|\vec{b}$ spectrum. The spectrum shown for $\vec{E}\|\vec{c}$ was taken on a polished *a* face. As a check on the quality of this face, we also recorded the $\vec{E}\|\vec{b}$ spectrum and found it to be identical to that

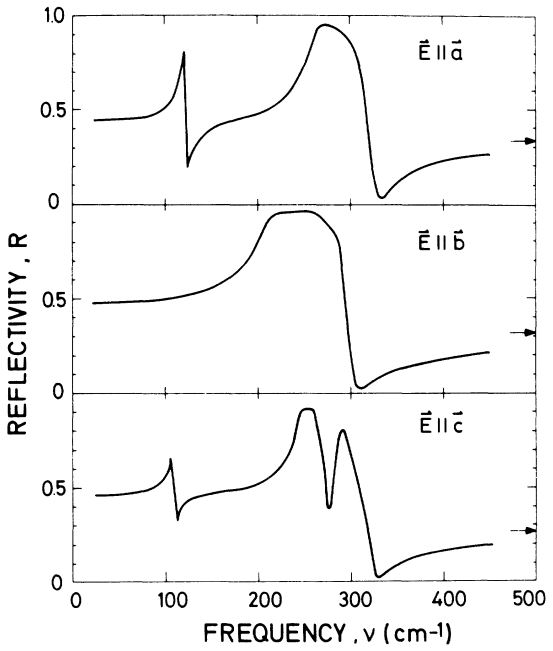

FIG. 2. Experimental reflectivity of GeS in all three principal polarizations from 20 to 450 cm^{-1} at 300 °K. The arrows at the right-hand side indicate the final values of reflectivity reached at 4000 cm^{-1}.

recorded on a cleavage face. Thus, the somewhat inferior quality of the polished surface presents no difficulties at these long wavelengths.

In accordance with the group-theoretical predictions (see Fig. 1), we observe reststrahl peaks corresponding to one TO phonon for $\vec{E}\parallel\vec{b}$ and three TO phonons for $\vec{E}\parallel\vec{c}$. In the $\vec{E}\parallel\vec{a}$ polarization, however, there should again be three TO phonons whereas we observe only two clearly resolved peaks. An extensive search was made for the "missing phonon" by performing repeated reflectivity measurements for several different samples at room temperature and one sample at 77 °K. In addition, we performed transmission measurements over the 20–450-cm^{-1} range. In no case did we find any clear evidence of the third phonon. Preliminary model calculations for the lattice dynamics of GeS indicate that this phonon should lie in the 150-cm^{-1} range.[20] If this is the case, then it must have an extremely small oscillator strength. We feel it is more likely that there are two phonons contributing to the 250–320-cm^{-1} peak and that, either these phonons are nearly degenerate, or one of them is quite heavily damped. This point will be discussed further in Sec. III.

In order to obtain better values for ϵ_∞ from our Kramers-Kronig analysis, the reflectivity measurements were extended to 4000 cm^{-1} ($\lambda = 2.5$ μm) using a Perkin Elmer Model 180-grating spectrophotometer. The reflectivity in the 450–4000-cm^{-1} range is structureless and will not be displayed in a separate figure. The final values of reflectivity reached at 4000 cm^{-1} are indicated by arrows on the right-hand edge of Fig. 2.

C. Raman measurements

Raman spectra were taken at room temperature using the back-scattering geometry. A Spex Triple monochromator, equipped with standard photon counting electronics, was employed to measure the phonon frequencies. Neon emission lines were used to calibrate the systems to within 0.5 cm^{-1}. The symmetries of the modes were determined from polarization selection rules and measured on both cleaved (c) and mechanically polished (b and a) samples prepared as described in Sec. II A. The observation of minimal Rayleigh scattering, even at 10 cm^{-1} away from the laser line, indicated the good quality of the polished surfaces.

The 6471-Å line of a Kr^+ laser was used as the excitation source for all measurements reported here. Owing to the high absorption coefficient of GeS at this wavelength, the scattering volume was very small and our Raman intensities were therefore weak. Nevertheless, the photon-counting system was sufficiently sensitive to allow us to measure the Raman spectra with adequate signal-to-noise ratios (better than 2:1 in the worst case, and approximately 10:1 for the stronger lines).

The Raman spectra of GeS are presented in Fig. 3 for various scattering geometries. The notation $X(YZ)\bar{X}$ indicates the incident direction, polarization vector of the incident and scattered photons and direction of the scattered light, respectively. By comparison of Figs. 1 and 3 it is seen that 12 Raman-active phonons ($4A_g + 2B_{1g} + 4B_{2g} + 2B_{3g}$) are predicted on the basis of the D_{2h}^{16} symmetry and exactly 12 modes were observed. Two mode symmetries, A_g and B_{1g}, were measured on a cleaved c face. Although one would expect the four A_g modes to appear in any parallel-parallel polarization configuration (diagonal matrix elements in the Raman tensor), it was found that two measurements were required to determine all four modes. This is indicative of the inequality of the matrix elements of the Raman tensor. For the remaining two symmetries, B_{2g} and B_{3g}, the b and a polished faces, respectively, were used.

III. ANALYSIS AND DISCUSSION

A. Kramers-Kronig analysis and oscillator fits

Assuming constant reflectivity below 20 cm^{-1} and above 4000 cm^{-1} a Kramers-Kronig integration was performed giving the phase angle of the complex reflectivity. The optical constants were then

calculated by inverting Fresnel's formula for reflection. Figure 4 shows the real part ϵ_1, and imaginary part ϵ_2 of the complex dielectric function ϵ versus frequency from 0 to 500 cm^{-1}, as obtained from the Kramers-Kronig analysis. Barker[21] has emphasized the dangers and difficulties of associating particular structural features in ϵ_1 and ϵ_2 with phonon energies in cases where the

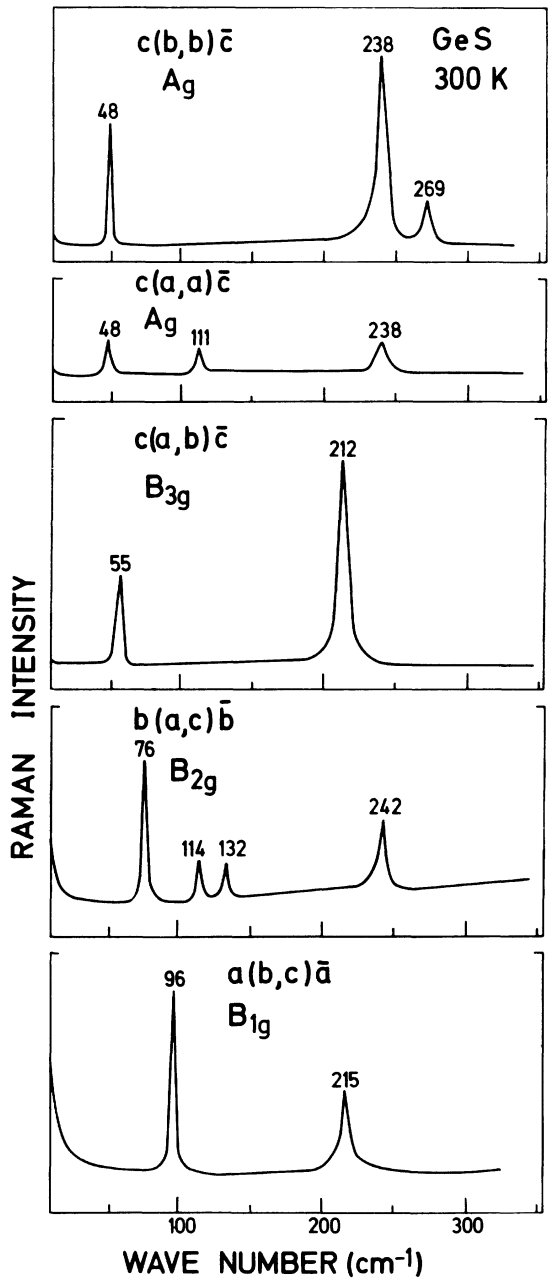

FIG. 3. Experimental Raman spectra for GeS at 300°K. The notation $x(y,z)\bar{x}$ indicates the incident direction of the exciting radiation, the polarization of the incident and scattered photons, and the direction of the scattered radiation, respectively.

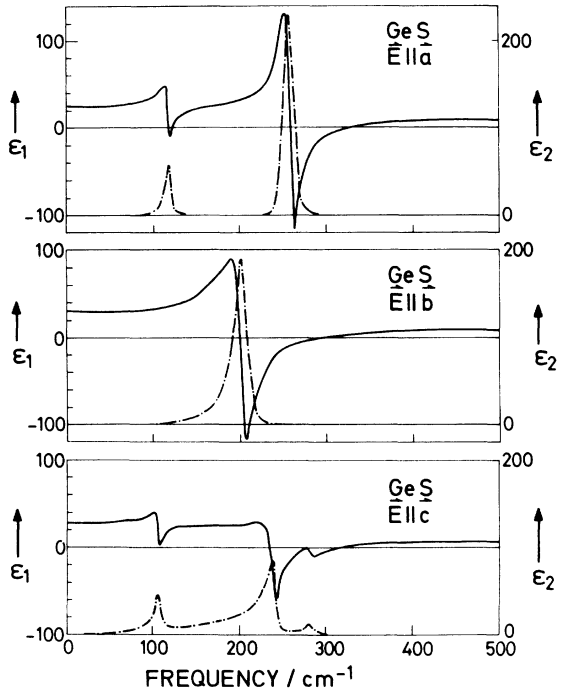

FIG. 4. The real ϵ_1 and imaginary ϵ_2 parts of the complex dielectric function of GeS as obtained from a Kramers-Kronig analysis of the reflectivity spectra shown in Fig. 2.

phonons are closely spaced and/or heavily damped. For present purposes, we adopt Barker's approximation[21] and assume that the maxima in the ϵ_2 spectra occur at the TO phonon frequencies and the above-resonance (positive slope) zero crossings of ϵ_1 occur at LO phonon frequencies. For the $\vec{E}\|\vec{c}$ polarization, there are two resonances for which ϵ_1 exhibits no zero crossings. In these cases, no truly longitudinal vibrations exist. Nevertheless, we have estimated where the zero crossings *would* occur if the damping were lower, thereby obtaining approximate LO frequencies. Using these definitions, the TO and LO phonon frequencies are tabulated in Table I along with values for the static and high-frequency dielectric constants, ϵ_0, and ϵ_∞. The values given for ϵ_∞ are the $\nu = 4000$ cm^{-1} values of ϵ_1.

B. Oscillator fits

Starting with the TO frequencies obtained from the Kramers-Kronig analysis, an oscillator model was constructed using the following expression for the complex dielectric function:

$$\epsilon(\omega) = \epsilon_\infty + \sum_j \frac{S_j^2}{\omega_j^2 - \omega^2 - i\gamma_j\omega} \quad , \tag{1}$$

where ω_j, S_j, and γ_j are, respectively, the position, strength and damping of the jth oscillator.

TABLE I. Phonon energies and dielectric constants for GeA as determined from a Kramers-Kronig analysis of the infrared reflectivity from 20 to 4000 cm^{-1}. All phonon energies are given in cm^{-1}. Two of the LO phonons for $\vec{E} \parallel \vec{c}$ are enclosed in parentheses to emphasize uncertainties in their values as discussed in the text.

	$\vec{E} \parallel \vec{a}$	$\vec{E} \parallel \vec{b}$	$\vec{E} \parallel \vec{c}$
TO_1	117.5	201.0	105.0
LO_1	123.5	298.0	107.0
TO_2	257.5	...	237.0
LO_2	325.0	...	(275.0)
TO_3		...	280.0
LO_3		...	(320.0)
ϵ_0	25.1	29.5	30.0
ϵ_∞	14.8	12.0	10.0

Oscillator parameters were chosen to obtain the best agreement between calculated and experimental reflectivities, with the sole constraint that the ω_j values should remain as close as possible to the TO frequencies given in Table I. We did not have access to a least-squares optimization program and the adjustment of parameters was done manually with the aid of a minicomputer equipped with a plotter which allowed us to plot calculated reflectivity curves as "overlays" on the experimental data. The fits which were obtained are shown in Fig. 5 and the corresponding oscillator parameters are given in Table II. Each of the reflectivity fits will now be discussed individually in greater detail.

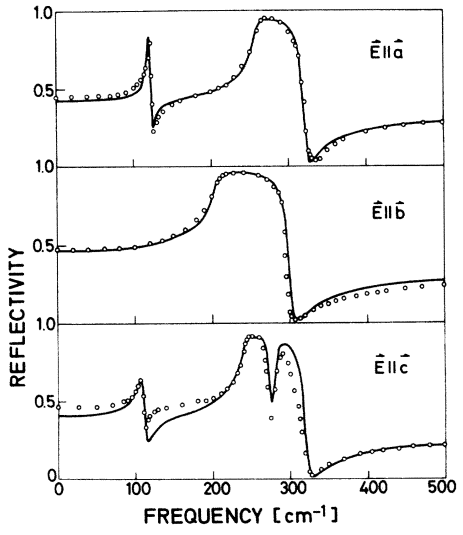

FIG. 5. Oscillator fits for the reflectivity spectra shown in Fig. 2 assuming independent oscillators with constant damping. The solid lines were calculated using the oscillator parameters given in Table II, and the points were taken from the experimental curves in Fig. 2.

For $\vec{E} \parallel \vec{a}$ the agreement between experimental and calculated reflectivity is quite satisfactory. It is noteworthy that this fit was obtained with only two oscillators despite the fact that three infrared-active phonons are predicted for this polarization by group theory. Equally good fits were obtained with a three-oscillator model, but only when extreme values were chosen for the parameters of the third oscillator (very low oscillator strength, strong damping, or near degeneracy with the second oscillator). In no case was a three-oscillator fit better than the two-oscillator fit shown in Fig. 5. By comparing Tables I and II it is seen that it was not necessary to change the oscillator energies from the values obtained from the Kramers-Kronig analysis, but there is a slight disagreement in the values for ϵ_0 and ϵ_∞.

For $\vec{E} \parallel \vec{b}$ the agreement between experimental and calculated reflectivity is again quite good. In this case, the best over-all agreement was obtained when the oscillator position was shifted to 205 cm^{-1} instead of being kept at the position indicated by the Kramers-Kronig analysis (201 cm^{-1}). It would appear, from a casual inspection of Fig. 5, that the fit in the 400–500-cm^{-1} range could be improved by simply lowering the assumed value for ϵ_∞ and raising the oscillator strength slightly to keep the reflectivity at lower frequencies from falling. This results in a very rapid degradation of the fit in the neighborhood of the reststrahl peak, however, and a worsening of the over-all fit. Similar comments apply to other small variations of the parameters which were attempted in the final stages of the fitting process.

The fit shown in Fig. 5 for $\vec{E} \parallel \vec{c}$ is substantially worse than those for $\vec{E} \parallel \vec{a}$ and $\vec{E} \parallel \vec{b}$. This result could have been anticipated from the ϵ_1 and ϵ_2 spectra obtained for $\vec{E} \parallel \vec{c}$ portion of Fig. 4 shows

TABLE II. Parameters used in the oscillator model for calculating the GeS reflectivity curves shown in Fig. 5. Frequencies, oscillator strengths, and damping constants are all expressed in units of cm^{-1}.

	$\vec{E} \parallel \vec{a}$	$\vec{E} \parallel \vec{b}$	$\vec{E} \parallel \vec{c}$
ω_1	117.5	205.0	105.0
ω_2	257.5	...	237.5
ω_3		...	280.0
S_1	160.0	790.0	200.0
S_2	695.0	...	630.0
S_3		...	160.0
γ_1	1.0	5.0	7.0
γ_2	5.0	...	7.0
γ_3	...	...	5.0
ϵ_0	22.7	27.9	20.9
ϵ_∞	13.5	13.0	10.0

TABLE III. Frequencies (in cm^{-1}) of Raman-infrared doublets which have been split in accordance with the predictions of Fig. 1.

$R(A_g)$	$ir(B_{1u})$	$R(B_{3g})$	$ir(B_{2u})$	$R(B_{2g})$	$ir(B_{3u})$
269	258	212	201	242	280
238	( )			132	238
111	118			114	105

that the resonances in ϵ_1 are extremely asymmetrical, and that ϵ_1 remains essentially flat between the first two resonances. This is quite unlike the behavior of simple independent oscillators, and leads us to conclude that a more sophisticated model (including frequency-dependent damping and coupling between the upper two oscillators) is necessary if better fits are to be obtained. Concerning the upper two oscillators in the $\vec{E}\|\vec{c}$ polarization, another point should be noted: The best over-all fit was obtained when the second oscillator had a normalized oscillator strength of $S_2' = S_2/\omega_2 = 630/237.5 = 2.653$. Comparing this with the second oscillator of the $\vec{E}\|\vec{a}$ polarization (for which $S_2' = 695/257.5 = 2.699$) one sees that these two oscillators are nearly identical. Thus, if it were not for the presence of the third oscillator ω_3 in the $\vec{E}\|\vec{c}$ polarization, the ω_2 oscillator would cause a reststrahl peak nearly identical to the one seen for $\vec{E}\|\vec{a}$. In particular, the ω_2 reststrahl peak would, by itself, extend to about 300 cm^{-1}. The sharp dip in reflectivity seen at 275 cm^{-1} is therefore *not* due to a coincidence between the ending of the ω_2 peak and the beginning of the ω_3 peak. Rather, it is caused by a partial cancellation between the negative ϵ_1 of the ω_2 oscillator and the positive ϵ_1 of the ω_3 oscillator. This point is mentioned simply to reemphasize the difficulty of determining LO phonon frequencies when the oscillators are so closely spaced that the ϵ_1 resonances begin to overlap.

C. Comparison of infrared and Raman mode frequencies

We are now in a position to compare the infrared and Raman frequencies and discuss the implications of our data in terms of interlayer force constants. Returning briefly to Fig. 1, it is seen that the introduction of interlayer coupling gives rise to three low-lying, Raman-active phonons, $1A_g + 1B_{2g} + 1B_{3g}$, which can be identified as rigid-layer modes[14,15] in which individual layers move against each other as units. In the present case, we can make the following identification: The A_g and B_{3g} phonons are shear modes in which adjacent layers move parellel to one another in the $\vec{a}$ and $\vec{b}$ directions, respectively, and the B_{2g} phonon is a compressive mode in which adjacent layers vibrate against one another in the $\vec{c}$ direction. From Fig. 3, the frequencies of these three rigid-layer modes are seen to be $\nu(A_g) = 48$, $\nu(B_{3g}) = 55$, and $\nu(B_{2g}) = 76$ cm^{-1}. Since the force constant of a classical oscillator is proportional to the square of the resonant frequency, these three frequencies can be used directly to adjust the interlayer force constants in a dynamical model. Again, referring to Fig. 1, it is seen that the interlayer interaction also causes splittings in the higher-energy modes such that for small splittings[14]

$$\nu_\pm = (\nu_0^2 \pm \Delta^2)^{1/2} \quad , \tag{2}$$

where ν_0 is the frequency in the absence of interlayer coupling and Δ is the shift caused by coupling. Table III contains the seven appropriate pairs of infrared and Raman-active phonons for convenient comparison of their splittings. In one case (the "missing" infrared-active phonon in the $\vec{E}\|\vec{a}$ polarization) no comparison is possible. Of the remaining six pairs, four show relatively small splittings (7–11 cm^{-1}) and two show splittings which are too large to be treated as perturbations. Following Zallen,[14] we can use Eq. (2) to estimate the ratio of intralayer to interlayer force constants. One expects that the values of Δ obtained from the splittings should be of the same order of magnitude as the rigid-layer mode frequencies reported above, and that the force-constant ratio should be given approximately by $(\nu_0/\Delta)^2$. Table IV shows the results of this sort of analysis obtained for the four weakly split pairs of phonons. Without specific knowledge of the eigenvectors for each vibrational mode, it is not possible to make detailed comments concerning these splittings or the strong splittings of the other two $B_{2g} - B_{3u}$ pairs. Nevertheless, a few qualitative observations are of interest. Consider the upper two pairs of phonons in Table IV ($A_g - B_{1u}$ and $B_{3g} - B_{2u}$). These are the highest-energy phonons and can thus be safely identified as two of the "NaCl-type" vibrations in which the Ge and S sublattices vibrate against one another. For these two cases, it is seen that Δ does, indeed, agree with the rigid-

TABLE IV. Values obtained for the frequency-splitting parameters of Eq. (2) for 4 pairs of Raman- and infrared-active phonons. The observed phonons with frequencies of ν_+ and ν_- would be degenerate, with frequencies ν_0, in the absence of interlayer coupling. The final column $(\nu_0/\Delta)^2$ is a rough measure of the ratio of intralayer to interlayer force constants for each pair of chonons. All frequencies are given in cm^{-1}.

Splitting	ν_+	ν_-	ν_0	Δ	$(\nu_0/\Delta)^2$
A_g-B_{1u}	269	258	264	54	24
B_{3g}-B_{2u}	212	201	207	48	19
B_{1u}-A_g	118	111	115	28	16
B_{2g}-B_{3u}	114	105	110	31	12

layer mode frequencies, and that the force-constant ratios are quite large (approximately 20:1). A force-constant ratio of 20:1 is certainly consistent with the exceptionally easy (001) cleavage of GeS, but is still small compared to the ratios obtained for many other "layer-type" compounds. Thus, for example, Zallen *et al.*[14] estimate (using the same "frequency-ratio" criterion as used here[22]) that the force-constant ratio in As_2S_3 is about 100:1.

Taking a slightly different approach, we can use the rigid-layer mode frequencies to estimate the ratios of specific force constants. Using the a direction as an example, the rigid-layer *shear* mode in this direction has a frequency of 48 cm^{-1}. In the absence of interlayer coupling, the highest-frequency intralayer vibration in the a direction would be 264 cm^{-1} (ν_0 from the top line of Table IV). This gives a force-constant ratio of $(264/48)^2 = 30$. Similar reasoning for the b direction gives a ratio of $(207/55)^2 = 14$. Because of the large splittings in the c direction, it is difficult to define an unshifted frequency for the intralayer vibrations. Taking 260 cm^{-1} as an average value, we obtain a ratio of intralayer to interlayer *compressive* force constants in the c direction of $(260/76)^2 = 12$.

IV. SUMMARY AND CONCLUSIONS

We have reported the results of infrared-reflectivity and Raman-scattering experiments for single-crystal GeS at 300 °K. These measurements enabled us to determine the $q = 0$ phonon energies of 18 of the 19 optically active phonons predicted by group theory. Our failure to observe the remaining phonon (one of the $3B_{1u}$ phonons; infrared active for $\vec{E} \| \vec{a}$ remains a puzzle for which we have no satisfactory explanation. It was shown that certain pairs of the infrared- and Raman-active phonons would be degenerate in the absence of interlayer coupling, and the relatively small splittings between many of these pairs indicates the importance (though not necessarily the dominance) of *layer* symmetry in determining the lattice vibrations in GeS. Crude estimates were given for the ratios of various pairs of intralayer and interlayer force constants, yielding values in the range 12:1–30:1. These values are a factor of 2–5 times smaller than corresponding estimates for other layer-type compounds, such as As_2S_3, As_2Se_3, MoS_2, and GaSe.[14,15,22] We therefore suggest that it is perhaps not appropriate to classify GeS as a truly layer-type compound but, rather, to consider it an intermediate case between layerlike and three-dimensional crystals. In this regard, it will be very interesting to study the group IV-VI isomorphs of GeS: GeSe, SnS, and SnSe, all of which should be more anisotropic (layerlike) than GeS.[11] The extent to which GeS exhibits three-dimensional behavior in its *electronic* properties has been discussed by Venghaus and Büchner[23] who performed electron energy-loss measurements and found no anisotropy in the ϵ_2 spectrum above 3 eV. This is in qualitative agreement with absorption measurements of Wiley *et al.*[10] which showed extreme anisotropy in the immediate region of the band gap but less anisotrophy at energies above 2 eV.

ACKNOWLEDGMENTS

The crystals used in this study were grown by E. Schönherr and W. Stetter and prepared for measurement by R. Berka and G. Fröhlich. Measurements utilizing the Fourier spectrometer were performed by W. König. Throughout the course of this work, we have benefitted from many helpful discussions with H. Bilz, M. Cardona, A. Frey, W. Kress, H. J. Queisser, and R. Zeyher. Finally, one of us (JDW) would like to thank the Alexander von Humboldt Foundation for making possible a one-year visit at this Institute.

---

*Work performed while on leave-of-absence from Bell Telephone Laboratories, Murray Hill, N. J. 07974.

†Present address: Dept. of Electrical and Computer Engineering, University of Wisconsin, Madison, Wisc. 53706.

‡Present address: Polytechnisches Institut, Dr. W. Ständer, 75 Karlsruhe.

[1]T. Yabumoto, J. Phys. Soc. Jpn. 13, 559 (1958).

[2]A. Okazaki, J. Phys. Soc. Jpn. 13, 1151 (1958).

[3]K. L. Lider and L. E. Solov'ev, Fiz. Tverd. Tela 4, 1500 (1962) Sov. Phys.-Solid State 4, 1102 (1962).

[4]G. Handfield, M. D'Amboise, and M. Bourgon, Can. J. Phys. 44, 853 (1966); 46, 3546 (1967).

[5]S. G. Karbanov, P. Petrov, and S. Ivanov, Dokl. Bolg. Akad. Nauk. 23, 17 (1970).

[6]J. G. A. M. Van den Dries and R. M. A. Lieth, Phys. Status Solidi A 5, K171 (1971).

[7]V. V. Sobolev and V. I. Donetskikh, Izv. Akad. Nauk. SSSR-Neorg. Mat. 8, 688 (1972). [Inorg. Mater. 8(4), 599 (1972).]

[8]L. Stourac, M. Zavetova, and A. Abraham, in *Proceedings of the 12th International Conference on the Physics of Semiconductors, Stuttgart*, 1974, edited by M. A. Pilkuhn (Teubner, Stuttgart, 1974), p. 1012.

[9]J. D. Wiley, E. Schönherr, and W. Stetter, Verh. Dtsch. Phys. Ges. 5, 401 (1975).

[10]J. D. Wiley, A. Breitschwerdt and E. Schönherr, Solid State Commun. (to be published).

[11]N. Kh. Abrikosov, V. F. Bankina, L. V. Poretskaya, L. E. Shelimova, and E. V. Skudnova, *Semiconducting II-VI, IV-VI, and V-VI Compounds* (Plenum, New York, 1969), Chap. II.

[12]R. Zeyher, W. Kress, and A. Frey (unpublished).

[13]In this paper, the notation used for the crystallographic axes follows that of Refs. 2, 9, 10, and 12. Other authors have followed different conventions and care

should be excerised in comparing results.

[14]R. Zallen, M. L. Slade, and A. T. Ward, Phys. Rev. B 3, 4257 (1971).

[15]R. Zallen, in *Proceedings of the 12th International Conference on the Physics of Semiconductors, Stuttgart* 1974, edited by M. H. Pilkuhn (Teubner, Stuttgart 1974), p. 621.

[16]E. A. Wood, Bell Syst. Technol. J. 43, 541 (1964).

[17]We are indebted to A. Frey for providing us with the information necessary for the construction of Fig. 1. See also Ref. 12.

[18]E. Schönherr and W. Stetter, J. Cryst. Growth 30, (1975).

[19]Monsanto Chemical Corp.

[20]R. Zeyher (private communication).

[21]A. S. Barker, Jr., Phys. Rev. 136, A1290 (1964).

[22]Actually, the ratio of intralayer to interlayer force constants is not given accurately by $(\nu_0/\Delta)^2$. For a more sophisticated analysis which takes account of the different reduced masses involved in the intralayer and interlayer vibrations see R. Zallen and M. Slade, Phys. Rev. B 9, 1627 (1974). From results presented by Zallen and Slade, we would assume that our values of $(\nu_0/\Delta)^2$ overestimate the force-constant ratios by a factor of 1.5–2.

[23]H. Venghaus and U. Büchner, Phys. Status Solidi (to be published).